

Adsorption and onset of lubrication by a double-chained cationic surfactant on silica surfaces

Laurence Serreau, Muriel Beauvais, Caroline Heitz, and Etienne Barthel

*Laboratoire Surface du Verre et Interfaces, UMR 125, CNRS/Saint-Gobain, 39
quai Lucien Lefranc, B.P. 135, F-93303 Aubervilliers cedex, France*

Abstract

In the context of glass fiber manufacturing the onset of lubrication by a C₁₈ double-chained cationic surfactant has been investigated at high normal contact pressures. Comparison with adsorption kinetics demonstrates that lubrication is not directly connected to the surfactant surface excess but originates from the transition to a defect-free bilayer which generates limited dissipation. The impact of ionic strength and shear rate has also been studied.

Key words: Friction, lubrication, silica, glass, surfactant, surface modification

PACS:

Email address: etienne.barthel@saint-gobain.com (Laurence Serreau,
Muriel Beauvais, Caroline Heitz, and Etienne Barthel).

1 INTRODUCTION

2 During glass fiber manufacturing, the high friction characteristic of silicate
3 surfaces in water results in surface damage and eventually prejudices the ten-
4 sile strength of the fibers. The necessary lubrication can be imparted through
5 an aqueous dispersion (sizing) which is applied at the initial stage of the glass
6 fiber manufacturing process. The sizing serves many purposes but double-
7 chained cationic surfactants (softeners) are often added to this dispersion to
8 participate in lubrication. However, it is well known that adsorption of sur-
9 factants proceeds slowly [1,2], especially for long-chained amphiphiles [3]. The
10 question we address in this paper is the kinetics of lubrication: once surfactant
11 adsorption has started, when will lubrication be effective ?

12 It is expected that the answer depends upon the mechanical loading and the
13 friction velocity in a complex manner. In practice, the typical drawing speed
14 is several meters per second, but the contacts between the several hundred
15 glass filaments within one fiber will slide at much slower velocities, which can
16 be in the range of millimeters per second or lower. The filaments slide against
17 each other in the presence of the sizing which initiates both adsorption and
18 lubrication. Such are the operating conditions we emulate in the present study.

19 Numerous studies have been conducted on the contact and also the friction
20 properties of surfactant covered surfaces. For practical reasons, the bulk of
21 the literature is devoted to short, single chain surfactants, which exhibit
22 faster equilibration [4,5,6]. Simultaneously, because of their relevance in bi-
23 ological applications, numerous papers deal with the adsorption of lipids. In
24 particular the structure of the surface aggregates and the mechanical response

25 of these insoluble double-chained surfactants have been studied in great de-
26 tails [6,7,8,9,10].

27 In this paper, we investigate the early stages of lubrication just after immersion
28 of silica surfaces in an aqueous dispersion of a typical double-chained (2 C₁₈)
29 cationic surfactant. The surfactant dispersion was investigated by Small Angle
30 Xray Scattering (SAXS) and Static Light Scattering (SLS) and the adsorption
31 kinetics on silica surfaces by Attenuated Total Reflection (ATR) Fourier Trans-
32 form Infrared (FTIR) spectroscopy. Using atomic force microscopy (AFM) and
33 macroscopic friction tests, we have measured the contact properties (repulsive
34 barrier, adhesion and friction) of macroscopic silica surfaces in the initial stages
35 of adsorption as a function of time after immersion. The results highlight the
36 impact of the adsorption kinetics and the changes of the surfactant configura-
37 tion during the early stages of adsorption. The picture which emerges is that
38 of a gradual transition from a disordered adsorbed layer with high friction to
39 a lubricating defect-free bilayer. Shear is shown to play a role in the transition
40 to the lubricating state.

41 **2 EXPERIMENTAL SECTION**

42 *2.1 Materials*

43 The double-chained cationic surfactant 1-methyl-2-noroleyl-3-oleic acid-aminoethyl-
44 imidazolium methosulfate (DOAIM, Figure 1) in isopropanol (25% wt) is
45 obtained from Goldschmidt Rewo GmbH & Co.,(Germany) and used as re-
46 ceived. The molecular weight is 740 g/mol and the density 0.97 g/cm³. The
47 CMC with isopropanol measured by surface tension is 1×10^{-5} M. The chain

48 melting temperature is 46°C as measured by DSC, in agreement with the val-
49 ues obtained for similar compounds [11]. All the experiments were performed
50 at ambient temperature.

51 Solutions of DOAIM at 5×10^{-4} M or 1×10^{-3} M were prepared in milli Q water
52 with 24 hours gentle stirring after evaporation of the isopropanol at 60C. Most
53 experiments were carried out at natural $\text{pH} \simeq 4.6$. In a set of experiments, the
54 ionic strength was varied with acetic acid/sodium acetate while maintaining
55 constant $\text{pH}=4.5$. Such concentration and pH conditions are typical for actual
56 sizing formulations.

57 *2.2 Methods*

58 *2.2.1 Equilibrium characterization*

59 The SAXS experiments were performed in a Kratky set-up (Anton Paar) with
60 a Cu K_{α} source (0.1542 nm) and a linear gas detector placed at 23 cm from
61 the source. The SLS experiments were performed on a Malvern Zetasizer 3
62 equipped with an He-Ne laser (633 nm), a photomultiplier and a goniometer.
63 The same piece of equipment was used to measure the zeta potential by elec-
64 trophoretic mobility in a liquid cell. The laser interferometric comb method
65 was used. The test system was 200 nm diameter silica particles (Stöber syn-
66 thesis). Adsorption at a given concentration was carried out by dilution from
67 a 10^{-4} M surfactant solution followed by 5 hour equilibration time. Surface
68 tension was measured by the Wilhelmy plate method.

70 Adsorption kinetics were measured by FTIR spectroscopy in the ATR mode
71 using a Nicolet Nexus 670 spectrometer equipped with a MIR source, a KBr
72 beamsplitter and a MCT-A detector. The experiments were carried out on
73 a germanium internal reflection element (trapezoidal, $50 \times 10 \times 1 \text{ mm}^3$, 45° inci-
74 dent angle) covered on the larger side by a silica layer $\simeq 7$ nm thick deposited by
75 magnetron sputtering. Before use, the surfaces were cleaned with a sequence
76 of detergent solution, deionized water, acetone and absolute ethanol for 15
77 minutes in an ultrasonic bath, followed by a final UV/Ozone treatment for
78 1 h. After cleaning, the wafer was introduced in the internal multi-reflection
79 cell which was immediately assembled and aligned in the sample compartment
80 of the spectrometer. A peristaltic pump and a three-way valve were used to
81 circulate either the pure solvent or the surfactant solution through the flow
82 cell. Spectra were taken at a resolution of 4 cm^{-1} for 8, 32 or 128 scans. A
83 background spectrum was collected after the cell was filled with water, before
84 the surfactant solution was pumped in. Following Harrick [12,13,14,15,16], the
85 amount of adsorbed surfactant can be quantified from the absorbance of some
86 vibration band of the molecule. In our case we have followed the evolution
87 of the CH_2 bands between 2800 and 3000 cm^{-1} . Absorbance of the vibration
88 band ν_s (CH_2) at 2854 cm^{-1} is used to determine the surface excess as a
89 function of time. This band has been chosen because it is less affected by the
90 baseline drift associated with the strong band of water in the range 3200 - 3300
91 cm^{-1} . The surface excess Γ is calculated from [12,14]

$$92 \quad A = k\epsilon \left[\frac{c_s d_p}{2} + \Gamma \right] \quad (1)$$

$$d_p = \frac{\lambda}{2\pi n_1 \sqrt{\sin^2 \theta - \left(\frac{n_2}{n_1}\right)^2}} \quad (2)$$

$$k = \frac{n_2 E_0^2}{n_1 \cos \theta} N \quad (3)$$

95 where d_p is the penetration length of the evanescent wave, λ the wavelength,
 96 N the number of internal reflections, E_0 the electric field amplitude, n_1 and
 97 n_2 the refractive index of the germanium and the solution respectively, θ the
 98 incident angle, A and ϵ respectively the absorbance and molecular extinction
 99 coefficient of the vibration band considered, and c_s the concentration of the
 100 absorbing species in solution. Assumption is made that c_s is not modified by
 101 adsorption. In practice N and E_0 cannot easily be determined so that k is
 102 determined from relation (1) by a calibration with a non adsorbing compound
 103 of known extinction coefficient (tert-butanol).

104 *2.2.3 AFM Surface forces measurement*

105 AFMs have been used for surface forces measurements in various environ-
 106 ments [17,18,19]. Here the experiments were performed on a Nanoscope III
 107 (Digital Instrument) with a silicon nitride tip using a liquid cell. Prior to the
 108 experiment, the tip was cleaned by irradiation for 60 minutes in a UV-ozone
 109 flow. A typical AFM experiment starts with a control of the tip shape quality
 110 and the silica surface cleanliness by measuring interaction forces between the
 111 AFM tip and the silica surface in milli-Q water. The DOAIM solution is then
 112 introduced and the surface forces profiles between tip and silica substrate are
 113 recorded every 3 minutes.

114 2.2.4 Friction experiments

115 Friction experiments have been performed on two reciprocating ball-on-plate
116 tribometers: for low pressure friction measurements, a home built millitribome-
117 ter with a 50 mN load range and a 0.02 mms^{-1} maximum sliding velocity was
118 used; for a larger friction velocity range, a commercial (Plint T79) tribometer
119 with sliding velocity ranging from 0.01 to 10 mms^{-1} . However, for this lat-
120 ter equipment, the normal load ranges between 0.1 and 20 N which results
121 in larger mean pressures. The plate is a silica, 2 mm thick substrate optically
122 polished on both sides (GE quartz). The ball is a fused silica sphere made from
123 silica rods (GE quartz). The end of the rod was melted with a blowtorch until
124 a molten droplet of glass formed with a radius of 2 to 4 mm . Both surfaces
125 were cleaned before use with a detergent-water-absolute ethanol sequence for
126 15 minutes in an ultrasonic bath.

127 To emulate lubrication in the presence of the sizing, the friction experiments
128 were all conducted in the presence of the aqueous surfactant dispersion, in-
129 side a liquid cell. It is also important to note that to minimize and control
130 the impact of shear, the typical friction experiments were not conducted as
131 continuous runs as is usually done for such measurements: on the contrary, un-
132 less otherwise stated, the surfaces were brought into contact every 5 minutes
133 for a series of two cycles only, typically lasting a few seconds and were then
134 separated again (Fig. 2). The friction force was measured by averaging on the
135 second cycle. When separated, care was taken that the silica surfaces remained
136 immersed in the solution until the next measurement. For each experiment,
137 the friction coefficient was first measured between surfaces immersed in pure
138 water. The water was then removed and replaced by the solution under study.
139 The first point in each friction graph is therefore the friction coefficient in pure

140 water.

141 **3 Results**

142

143 *3.1 Characterization of the solution and adsorption*

144 The pure surfactant system (after extraction of the isopropanol) is optically
145 birefringent. The SAXS diffractogram exhibits one single, fine Bragg peak
146 (Fig. 3) typical for an L_β phase. The repeat distance is 3.31 nm. After di-
147 lution in water (1 M), the system exhibits shear induced birefringence which
148 persists over days. In the SAXS diffractogram, a series of equally spaced peaks
149 is recorded (Fig. 3). These features are also typical for a lamellar phase. The
150 first order diffraction peak has moved to smaller wave vector and the repeat
151 distance has increased to 7.85 nm, which is fully consistent with the 7.65 nm
152 value expected for dilution of the lamellar phase to 1 M. Upon further dilu-
153 tion the Xray signal and the optical birefringence is lost. Around 1×10^{-3} M,
154 well above the CMC, the bilayer conformation is also evidenced optically by
155 the presence of multilamellar vesicles. At lower concentrations, SLS exper-
156 iments were carried out. The scattered intensity recorded for 2.5×10^{-3} and
157 1.0×10^{-4} M are displayed on Fig. 4. Beyond the quadratic behaviour for small
158 diffusion wave vectors, the static correlation function exhibits a moderate de-
159 cay. The full shape of the correlation function is consistent with extended
160 disks [20] as expected for large dilutions where the correlation between lamel-
161 lae is lost. The measured correlation length are 310 and 550 nm for 2.5×10^{-3}

162 and 1.0×10^{-4} M, showing that the materials behaves as sheets at lengthscales
163 smaller than the correlation length. In conclusion, the surfactant solution ex-
164 hibits a lamellar phase resulting from the bilayer association of the individual
165 surfactant molecules and the bilayer structure is preserved upon dilution.

166 From the surface tension as a function of concentration, we determined a criti-
167 cal micelle concentration $\text{CMC} = 9 \times 10^{-6}$ M and an area per head $A_H = 0.71 \text{ nm}^2$.
168 The results of the zeta potential measurements at natural pH are displayed on
169 Fig. 5. The zeta potential of the bare silica spheres is found at the expected
170 -60 mV value. Upon adsorption, the surface charge decreases and is finally
171 reversed at the point of zero charge $\text{PZC} = 5 \times 10^{-6}$ M well below the CMC.
172 This charge reversal behavior is characteristic for the adsorption of a bilayer
173 at the surface.

174 3.2 Friction – Time effect

175 A first series of friction experiments were carried out at low contact pressures
176 (concentration $C = 10^{-3}$ M, natural pH, sliding velocity $v = 0.014 \text{ mms}^{-1}$, mean
177 contact pressure $P_m = 90 \text{ MPa}$, Figure 6). The typical friction coefficient of
178 silica surfaces immersed in pure water is 0.6 ± 0.1 with a variability due to
179 surface preparation. Typical friction coefficients after five minutes of immer-
180 sion in the DOAIM solution ($C = 10^{-3}$ M) are down to 0.50 which indicates
181 negligible (though measurable) lubrication. On the other hand, if the surfaces
182 are first immersed 15 hours in a solution of DOAIM (10^{-3} M) before the fric-
183 tion experiment starts (procedure C) then the measured friction coefficient
184 is lower than 0.1, and sometimes reaches 0.03, revealing fully lubricated sur-
185 faces. Similar results are recorded for $C = 5 \times 10^{-4}$ M. The long equilibration

186 time in procedure C is typical for surfactant lubrication experiments [21,22].
187 A friction coefficient of about 0.1 or lower is usual for surfactant lubrication,
188 especially for double-chained surfactants with long chains [8,23,24]. However,
189 when the same friction experiment starts immediately after immersion in the
190 surfactant solution (procedure A), the friction coefficient decreases to reach
191 the low friction value (about 0.05) after only *ca* 2 hours. The transition is
192 not linear with time. With repeated friction tests carried out every 5 min
193 we observe an initial plateau at the high friction value around 0.5-0.6, which
194 typically lasts 1 hour before the friction coefficient starts to decrease by one
195 order of magnitude down to values around 0.05. These results exemplify the
196 fact that lubrication with double-chained surfactants is not instantaneous but
197 starts after an induction period.

198 *3.3 AFM surface forces measurements*

199 In the AFM force measurements, the force vs distance curve (Figure 7, inset)
200 first displays a repulsive long range interaction, followed by a steeper repulsive
201 interaction starting around 10 nm. The former has not been quantified due to
202 the low signal to noise ratio but the results are consistent with the electrostatic
203 double layer interaction demonstrated by the zeta potential measurements
204 (Fig. 5). The latter is due to the mechanical compression of the bilayer. Then,
205 for distances close to 3-4 nm, the AFM tip jumps into contact. This jump-
206 in distance of 3-4 nm is close to the thickness of a DOAIM bilayer. Such
207 a behaviour is well-known in the literature [4,25,26,27]. The jump-in force,
208 defined as the repulsive force at jump-in, is an estimate of the mechanical
209 resistance of the bilayers. Pulling the tip back induces the rupture of the

210 tip-surface contact: a negative force is registered which signals adhesion (not
211 shown on the inset). The amplitude of this pull-out force is a measure of the
212 tip-surface adhesion energy [28,29]. The jump-in force in a solution of DOAIM
213 (1×10^{-3} M) has been measured as a function of time, as well as the pull-out
214 force (Figure 7). We note that the jump-in and the pull-out forces measured
215 here are tightly correlated, as already reported in the literature [21]. The
216 jump-in force (counted positive) increases as the magnitude of the pull-out
217 force (counted negative) decreases. They obey a time evolution similar to the
218 friction coefficient: in procedure A, it stays constant for about one hour before
219 the decrease to low friction; similarly jump-in and pull-out forces exhibit an
220 initial plateau before a transition around 60 min to equilibrium values with
221 large jump-in force and negligible adhesion. More complete results on the
222 adsorption isotherm measured by ellipsometry and the mechanical response of
223 the surfactant bilayer at equilibrium obtained with a Surface Forces Apparatus
224 will be published separately.

225 3.4 Adsorption kinetics of DOAIM

226 In this context, it is interesting to correlate the time evolution of the contact
227 properties with the amount of surfactant adsorbed on the surface (surface ex-
228 cess). A measurement of the adsorption kinetics (5×10^{-4} M, FTIR-ATR) is
229 shown on Figure 8. Two different regimes are observed and the data is rea-
230 sonably well fitted by a double exponential function with a fast time constant
231 $\tau_1=25$ min and a slow time constant $\tau_2=205$ min, leading to a pseudo-plateau.
232 At pseudo-saturation, the adsorbed amount is $6.2 \mu\text{molm}^{-2}$. Rinsing with re-
233 circulating water leads to little desorption, down to $5.5 \mu\text{molm}^{-2}$. The area

234 per molecule determined from surface tension measurements is 0.79 nm^2 . From
235 this value we conclude that at saturation, a full bilayer is formed at the sil-
236 ica surface. A comparison of Figures 6 and 7 with Figure 8 demonstrates that
237 during the induction period, when the friction coefficient is high and constant,
238 the adsorption of the surfactant is fast. When the transition to the lubricated
239 state occurs (procedure A), we can estimate that the surface excess is already
240 roughly as large as half a bilayer. From this observation we conclude that there
241 is no simple proportionality relation between the adsorbed amount and the
242 friction coefficient in this regime but that a more complex mechanism is called
243 for to explain the onset of lubrication. In order to gain a clearer view of this
244 mechanism, we have performed a series of experiments to probe the impact of
245 kinetic parameters on the lubrication of the surfaces.

246 *3.5 Impact of shear on the onset of lubrication*

247 We measured the friction when the experiment starts only three hours after
248 immersion in the solution (procedure B, Figure 6). In such conditions, the
249 adsorption is almost complete (the surface excess amounts to 85% of the max-
250 imum, Figure 8) and a lubricated surface is obtained following procedure A.
251 If lubrication were only controlled by the adsorption of the surfactant, then a
252 low friction coefficient would be expected, as with procedure C. In contrast, a
253 trend similar to procedure A is observed: after 3 hours of induction, we mea-
254 sure an initial value of the friction coefficient of approximately 0.5. Transition
255 towards a low friction coefficient is observed around 1.5 hours after the friction
256 experiment has started, and a low value (0.07) is reached about 2 hours after
257 the beginning of the friction experiment, that is a total of about 5 hours after

258 immersion. This result attests to the fact that shear accelerates the onset of
259 lubrication: low friction is obtained after 2 hours in procedure A, in which
260 friction is probed every 5 minutes, but only after 5 hours in procedure B,
261 where the system is completely at rest for the first 3 hours.

262 3.6 Ionic strength effect

263 Ionic strength also impacts the adsorption process. In the presence of salt (pH
264 4.5), the adsorption kinetics is much faster (Figure 8, inset) and for an ionic
265 strength of 2×10^{-2} M, half-coverage of the surface is reached within minutes.
266 Figure 9 shows the evolution of the friction coefficient with time (DOAIM
267 5×10^{-4} M, $P_m = 320\text{-}340$ MPa, pH=4.5) for different salt concentrations. The
268 experiments follow procedure A where friction starts immediately after im-
269 mersion. We observe that the transition towards low friction is considerably
270 faster, a trend similar to the adsorption kinetics. The initial friction plateau
271 has now been suppressed and the time to reach the lubricating state decreases
272 when the ionic strength increases. For the highest salt concentration, the ini-
273 tial value of the friction coefficient after 5 minutes of immersion is already
274 3 times lower than in pure water. Note that the friction spike to 0.2 which
275 follows the first low friction data point (Figure 9) is a reproducible feature pre-
276 sumably connected to more dissipative intermediate configurations towards a
277 fully lubricated surface. Similarly at high ionic strength the AFM force curves
278 demonstrate an almost instantaneous build-up of the repulsive force wall (not
279 shown).

280 3.7 *Sliding velocity*

281 We have demonstrated in section 3.5 that shear accelerates the transition to
282 the lubricated state. A final set of experiments aims at exploring the im-
283 pact of *shear rate*. Friction experiments at different sliding velocities were
284 performed ($P_m=320-340$ MPa) following procedure A. For the lower velocity
285 (0.01 mms⁻¹), the global evolution is similar to the evolution recorded at lower
286 mean pressure in contact (90 MPa): the high (0.53) initial friction coefficient
287 decreases with time to reach a stable value of 0.06. However, we can perform
288 experiments in a wider velocity range only at higher loads (section 2.2.4). This
289 is why the transition towards low friction coefficient is achieved after 5 hours
290 instead of 2. For high velocities, the equilibrium configuration is reached much
291 faster, within 5-10 minutes. Figure 10 summarizes the main effects of the slid-
292 ing velocity on the initial and final values of the friction coefficient. Note that
293 the magnitude of the lubrication effect also decreases, since the value of the
294 friction coefficient of silica surfaces in pure water decreases with the sliding
295 velocity [30].

296 4 Discussion

297 4.1 *The generic lubricating state*

298 In the lubricated state, the friction coefficient is as low as 0.05, as observed for
299 instance in procedure C, after a 15 hour adsorption period. For the types of
300 loading used here, the mean normal pressures in the contact are significantly
301 larger than typical hemifusion thresholds for double-chained C₁₈ surfactants

302 (several 10 MPa) [31]. As a result, hemifusion of the bilayers present on both
303 surfaces occurs and this low value for the friction coefficient results from the
304 friction between two hydrocarbon monolayers (Figure 11 b'). In this lubricated
305 state, the average interfacial shear stress τ is of the order of 20 MPa and is little
306 affected by the sliding velocity. Such a value is typical for monolayer-monolayer
307 contacts in air [24] and is consistent with an approximate model connecting
308 friction and adhesion hysteresis $\Delta\gamma$ [23]. Indeed it has been proposed that

$$309 \quad \tau \simeq \Delta\gamma/\delta \quad (4)$$

310 where δ is a molecular dimension. Reasonable values are $\Delta\gamma \simeq 10 \text{ mJm}^{-2}$ and
311 $\delta \simeq 1 \text{ nm}$ [24], so that $\tau \simeq 10 \text{ MPa}$. Friction between the outermost surfaces of
312 the two pristine bilayers would lead to much lower friction coefficients: values
313 one order of magnitude lower, as low as 0.004, were reported for instance for
314 gemini surfactants [22].

315 *4.2 Organisation during adsorption*

316 As amply demonstrated by our present results, this configuration is not readily
317 obtained upon adsorption from the solution. Indeed, the equilibrium config-
318 uration in the bulk is usually different from the equilibrium configuration of
319 the surfactant aggregates adsorbed on a surface and the same surface excess
320 may lead to very different surfactant conformations, with either dissipation
321 and friction or lubrication. Subtle effects control the surfactant conformation
322 after adsorption [32,33,34,35,36].

323 This is especially true when the interaction is strong, which is the case when
324 surface and surfactant are oppositely charged: for cationic surfactants, the

325 electrostatic interaction with the negatively charged silica surface results in
326 fast initial adsorption (Fig. 8). After this first adsorption stage, reorganization
327 is required. For example, Chatteraj and Biswas [2] observed two characteris-
328 tics times for the adsorption kinetics of short-chained cationic surfactants on
329 silica surfaces. The mechanism they propose is as follows: in the first step, sur-
330 factant molecules from the bulk diffuse to the surface and adsorb quickly with
331 random orientation onto the silica surface; in the second step, the crowded
332 molecules tend to re-orient in a regular fashion leading to the formation of ad-
333 sorbed patches of surface micellar aggregates. Such configuration changes will
334 create more vacant spaces for further adsorption of surfactant from the bulk to
335 the surface. Similarly, for adsorption of CTAB *above* the cmc on mica surfaces,
336 Chen *et al.* [1] propose a slightly different model where micelles adsorb directly
337 on the surfaces and subsequently reorganize. The idea is supported by the fact
338 that the same density of molecules is measured in the adsorbed layer and in
339 the micelles in solution. DOAIM, as many double-chained C_{18} surfactant, is
340 dispersed as bilayers as further demonstrated by the present optical, SAXS
341 and SLS results. An adsorption process similar to lipid vesicle deposition must
342 therefore be considered: the charged vesicles present in the solution will adsorb
343 quickly as patches of bilayers and in an uncorrelated way [38,39]. Rearrange-
344 ment must proceed before a defect-free bilayer is obtained [15]. This scenario
345 parallels the mechanism proposed by Chen [1] but here the rearrangement is
346 expected to be slower: the characteristic times for adsorption are considerably
347 larger than for short chain surfactants [2,4] since for long chain surfactants,
348 below the chain melting temperature, reorganization is hampered by the slow
349 dynamics [3].

350 *4.3 Bilayers, depletion and contact properties*

351 The defective nature of the surfactant layer in the initial stage of adsorp-
352 tion strongly impacts its mechanical response. SFA experiments have shown
353 that lipid bilayers exhibit a smaller jump-in force and a larger pull-out force
354 when depleted, *i.e.* depletion facilitates hemifusion and increases adhesion [21].
355 Along the same line of thought, hemifusion in the SFA has been shown to corre-
356 late with defect density (monolayer or bilayer holes) as identified by AFM [40].
357 The defect density was controlled by the deposition pressure in the Langmuir-
358 Blodgett trough. Similar studies have been reported for the mechanical re-
359 sponse of lipid bilayers measured by AFM as a function of surface excess.
360 AFM experiments have shown that depletion [8] and ionic strength [6] impact
361 friction. The results were somehow discussed in terms of packing density. For
362 lipid bilayers, an interesting suggestion is that the reduced stability results
363 from the increased hydrophobic interactions between depleted bilayers [21],
364 not from a simple decrease in the density. Similarly, for shorter single-chained
365 surfactant it has also been observed either by SFA or AFM force measure-
366 ments that near the CMC, when the surfaces are pushed to bilayer contact,
367 the jump-in force increases with surfactant concentration while the adhesion is
368 maximum for monolayer coverage [16,41]. A connexion between micellization
369 energy and mechanical resistance at equilibrium has also been established [27].

370 These observations all converge to demonstrate that an increase in the packing
371 density of molecules in the outer layer of the bilayer leads to enhanced stability
372 and reduction of adhesion. In the present experiments the results demonstrate
373 an increase of the jump-in force and a reduction of adhesion as a function of
374 time (Fig. 7). For DOAIM adsorbed at concentrations significantly larger than

375 the CMC, the initial conformation is characteristic of frustrated aggregates
376 adsorbed at the surface (Fig. 11, a), which we loosely call defective bilayer.
377 Our results are in complete agreement with the picture of a gradual healing
378 of the initially defective bilayer.

379 *4.4 Friction and onset of lubrication*

380 Initially, before the defect-free bilayer is formed, a large friction coefficient is
381 recorded, around 0.5. Compared to the bare silica-silica friction coefficient,
382 this value demonstrate a very moderate impact of the adsorbed surfactant.
383 We suggest that this sizeable interfacial shear results from the dissipation
384 which accompanies the deformation of the aggregates present at the surface.
385 These deformations may be transitions from bilayer to tilted bilayer, aggre-
386 gate ruptures, etc (Fig. 11, a'). Defective bilayers give rise not only to easier
387 hemifusion and enhanced adhesion, but also to friction because they allow for
388 more deformation at the molecular scale. The results are similar to the large
389 friction recorded for lipid bilayers in AFM experiments when a second me-
390 chanical transition threshold is reached, well above hemifusion, and for which
391 "direct surface contact" is evoked [6,8,38].

392 The decrease towards low friction is typically observed after 1 hour (Fig 6).
393 In parallel the surface forces exhibit a decrease in the adhesion force and
394 the repulsive jump-in force becomes more pronounced (Fig. 7). This trend we
395 connect with the organization at the surface which evolves to a structure closer
396 to a more ordered, stable, bilayer exposing fewer hydrophobic moieties. The
397 transition at the local scale from a defective towards a stable bilayer has been
398 completed. Indeed the friction (Fig. 6) and adhesion (Fig. 7) drops recorded

399 here are consistent with Eq. 4.

400 There remains to be explained why the transition is abrupt and does not di-
401 rectly correlate with the surface excess. It is possible that a critical flaw size
402 exists below which the pressure-induced transition to a tilted or disorganized
403 layer is prevented. This concept parallels the theory for bilayer stability [42,43].
404 If the flaw density is large enough, as occurs initially, the full surface induces
405 dissipation through aggregate edges. It is only when sufficient healing has
406 occurred and some defect-free patches have formed that the overall friction
407 coefficient decreases. In this scheme, the lubricated state results from stabili-
408 sation of the surfactant layer through healing of the larger defects.

409 The transition towards the lubricated state occurs faster in the presence of
410 salt, because ionic strength screens long range electrostatic double layer in-
411 teractions and facilitates rearrangement. Similarly, we have observed that the
412 transition towards lubricating state occurs earlier in time when the system
413 is submitted to friction immediately after immersion. Higher sliding velocity
414 also accelerates the transition. We conclude that shear and/or contact due to
415 the friction experiment itself favors the bilayer organization of the surfactant
416 between the two surfaces [41]. Indeed shear provides the symmetry breaking
417 driving force which promotes layering [44,45] as well as the mechanical energy
418 which activates structural transitions [46]. It favours surfactant accumulation
419 and lamellar ordering turning the adsorbed material into a fully formed bi-
420 layer [9,41].

421 5 Conclusion

422 The friction coefficient between millimetric silica surfaces was measured dur-
423 ing adsorption of a C₁₈ double-chained surfactant. A transition from high to
424 low friction is observed which parallels the contact properties measured with
425 the AFM. The results are not directly correlated to the surface excess. They
426 point to the role of the organisation of the surfactant into a defect-free bi-
427 layer for lubrication to be effective. Lubrication is obtained faster at higher
428 ionic strength and under shear because both facilitate the bilayer organiza-
429 tion. We have also study the impact of addition of other surface active sizing
430 components such as silanes on surfactant lubrication. Strong effects have been
431 evidenced due to interaction and/or competitive adsorption, which have been
432 published separately [47].

433 6 Acknowledgements

434 We thank M. Clerc-Imperator and R. Roquigny for the SAXS experiments.

435 References

- 436 [1] Y.L. Chen, S. Chen, C. Frank, and J. Israelachvili. *J. Colloid Interf. Sci.*, 153
437 (1992) 244.
- 438 [2] S.C. Biswas and D.K. Chattoraj. *J. Colloid Interf. Sci.*, 205 (1998) 12.
- 439 [3] W. A. Hayes and D. K. Schwartz. *Langmuir*, 14 (1998) 5913.
- 440 [4] V. Subramanian and W. Ducker. *J. Phys. Chem. B*, 105 (2001) 1389.

- 441 [5] I. U. Vakarelski, S. C. Brown, Y. I. Rabinovich, and B. M. Moudgil. *Langmuir*,
442 20 (2004) 1724.
- 443 [6] G. Oncins, S. Garcia-Manyes, and F. Sanz. *Langmuir*, 21 (2005) 7373.
- 444 [7] R. M. Pashley, P. M. McGuiggan, B. W. Ninham, J. Brady, and D. F. Evans.
445 *J. Phys. Chem.*, 90 (1986) 1637.
- 446 [8] L. M. Grant and F. Tiberg. *Biophys. J.*, 82 (2002) 1373.
- 447 [9] K. Boschkova, A. Feiler, B. Kronberg, and J. J. Stalgren. *Langmuir*, 18 (2002)
448 7930.
- 449 [10] K. Boschkova, B. Kronberg, J. J. Stalgren, K. Persson, and M. Ratoi-Salagean.
450 *Langmuir*, 18 (2002) 1680.
- 451 [11] Y. Liu and D. F. Evans. *Langmuir*, 12 (1996) 1235.
- 452 [12] N.J. Harrick. *J. Phys. Chem.*, 64 (1960) 1110.
- 453 [13] R. P. Sperline, S. Muralidharan, and H. Freiser. *Langmuir*, 3 (1987) 198.
- 454 [14] M.-J. Azzopardi and H. Arribart. *J. Adhes.*, 46 (1994) 103.
- 455 [15] D. J. Neivandt, M. L. Gee, M. L. Hair, and C. P. Tripp. *J. Phys. Chem. B*, 102
456 (1998) 5107.
- 457 [16] P. K. Singh, J. J. Adler, Y. I. Rabinovich, and B. M. Moudgil. *Langmuir*, 17
458 (2001) 468.
- 459 [17] W. A. Ducker, T. J. Senden, and R. M. Pashley. *Langmuir*, 8 (1992) 1831.
- 460 [18] S. Sounilhac, E. Barthel, and F. Creuzet. *Appl. surf. sci.*, 140 (1999) 411.
- 461 [19] S. Sounilhac, E. Barthel, and F. Creuzet. *J. Appl. Phys.*, 85 (1999) 222.
- 462 [20] B. Zhmud and F. Tiberg. *Adv. Coll. Interface Sci.*, 113 (2005) 21.

- 463 [21] C. A. Helm, J. N. Israelachvili, and P. M. McGuiggan. *Biochem.*, 31 (1992)
464 1794.
- 465 [22] C. Drummond, J. Israelachvili, and P. Richetti. *Phys. Review E*, 67 (2003)
466 066110–1–16.
- 467 [23] S; Yamada and J. Israelachvili. *J. Phys. Chem. B*, 102 (1998) 234.
- 468 [24] W. H. Briscoe, S. Titmuss, F. Tiberg, R. K. Thomas, D. J. McGillivray, and
469 J. Klein. *Nature*, 444 (2006) 191.
- 470 [25] J. J. Adler, P. K. Singh, A. Patist, Y. I. Rabinovich, D. O. Shah, and B. M.
471 Moudgil. *Langmuir*, 16 (2000) 7255.
- 472 [26] Y. I. Rabinovich, I. U. Vakarelski, S. C. Brown, P. K. Singh, and B. M. Moudgil.
473 *J. Colloid Interface Sci.*, 270 (2004) 29.
- 474 [27] Y. I. Rabinovich, S. Pandey, D. O. Shah, and B. M. Moudgil. *Langmuir*, 22
475 (2006) 6858.
- 476 [28] J. N. Israelachvili. *Intermolecular and Surface Forces*. Academic Press, San
477 Diego, 1992.
- 478 [29] E. Barthel. *J. Phys. D: Appl. Phys.*, 41 (2008) 163001.
- 479 [30] G. Di Toro, D. L. Goldsby, and T. E. Tullis. *Nature*, 427 (2004) 436.
- 480 [31] C. A. Helm, J. N. Israelachvili, and P. M. McGuiggan. *Science*, 246 (1989) 919.
- 481 [32] S. Manne and H. E. Gaub. *Science*, 270 (1995) 1480.
- 482 [33] E. J. Wanless and W. A. Ducker. *J. Phys. Chem.*, 100 (1996) 3207.
- 483 [34] R. E. Lamont and W. A. Ducker. *J. Am. Chem. Soc.*, 120 (1998) 7602.
- 484 [35] R. Atkin, V.S.J. Craig, E.J. Wanless, and S. Biggs. *Adv. Colloid Interf. Sci.*,
485 103 (2003) 219.

- 486 [36] S. Paria and K. C. Khilar. *Adv. Colloid Interf. Sci.*, 110 (2004) 75.
- 487 [37] R. P. Richter and A. Brisson. *Langmuir*, 19 (2003) 1632.
- 488 [38] R. P. Richter and A. Brisson. *Langmuir*, 19 (2003) 1632.
- 489 [39] R. P. Richter, R. Berat, and A. R. Brisson. *Langmuir*, 22 (2006) 3497.
- 490 [40] M. Benz, T. Gutschmann, N. Chen, R. Tadmor, and J. Israelachvili. *Biophys. J.*,
491 86 (2004) 870.
- 492 [41] R. W. Rutland and J. L. Parker. *Langmuir*, 10 (1994) 1110.
- 493 [42] B. N. J. Persson and E. Tosatti. *Phys. Rev. B*, 50 (1994) 5590.
- 494 [43] E. Barthel. *Thin Solid Films*, 330 (1998) 27.
- 495 [44] J. Zipfel, J. Berghausen, G. Schmidt, P. Lindner, P. Alexandridis, M. Tsianou,
496 and W. Richtering. *Phys. Chem. Chem. Phys.*, 1 (1999) 3905.
- 497 [45] Y. Li, Y. Golan, A. Martin-Herranz, O. Pelletier, M. Yasa, J. N. Israelachvili,
498 and C. R. Safinya. *Int. J. Thermophys.*, 22 (2001) 1175.
- 499 [46] M. Akbulut, C. Nianhuan, N. Maeda, J. Israelachvili, T. Grunewald, and
500 C. Helm. *J. Phys. Chem. B*, 109 (2005) 12509.
- 501 [47] M. Beauvais, L. Serreau, C. Heitz and E. Barthel. *J. Colloid Interf. Sci.* in
502 press, doi:10.1016/j.jcis.2008.11.036.

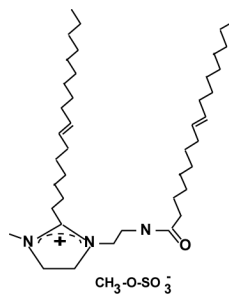


Fig. 1. Chemical structure of the DOAIM

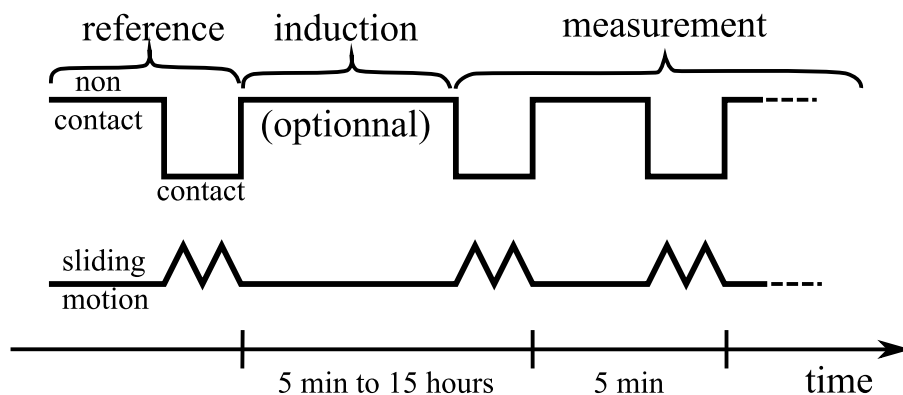


Fig. 2. Experimental protocol for the measurement of the kinetics of the onset of lubrication. The friction measurement proceeds by short friction runs separated by 5 min intervals during which the surfaces are kept far apart but submerged in the solution, in order to avoid drying problems. The measurement period is optionally preceded by an induction period during which the surfaces are kept far apart in the solution, without contact or friction measurement. The reference are individual runs performed initially in water and immediately after introducing the solution.

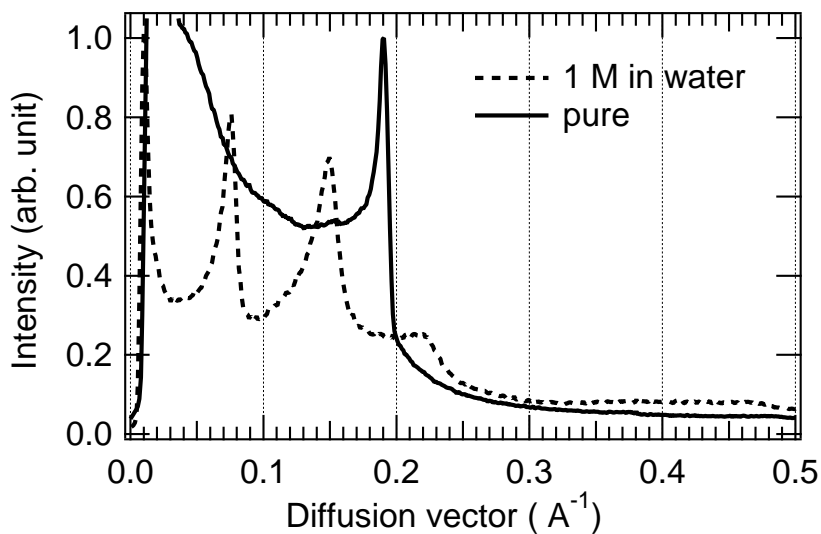


Fig. 3. X-ray diffraction spectra for pure and diluted DOAIM. The fine diffraction peaks shifting to smaller wave vector with dilution demonstrate the presence of a lamellar phase.

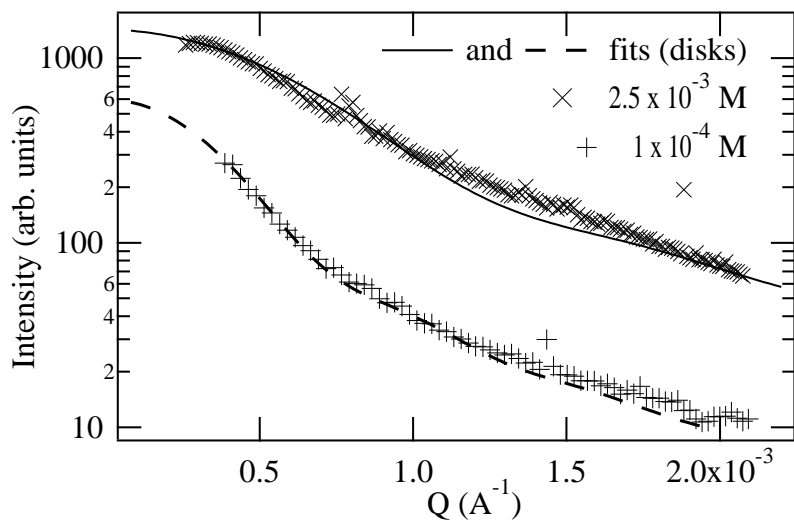


Fig. 4. Static light scattering of DOAIM at low concentrations with fits to disks shaped objects. The fits support the expected extremely diluted bilayer structure at these low concentrations.

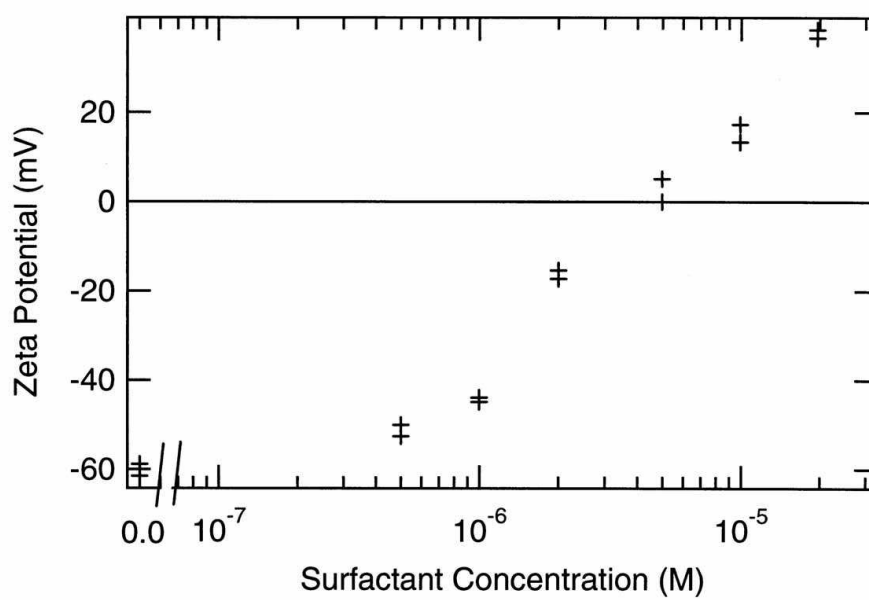


Fig. 5. Zeta potential as a function of surfactant concentration. The charge reversal is typical for the build-up of a surfactant bilayer at the surface.

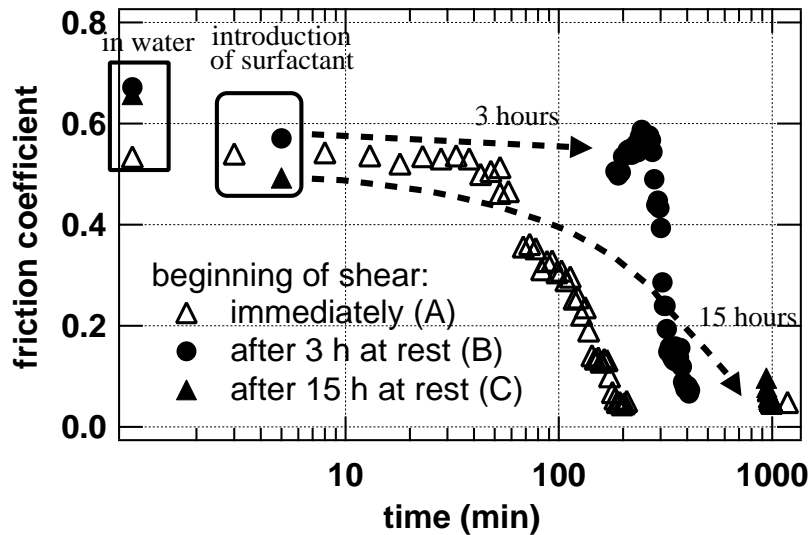


Fig. 6. Evolution of the friction coefficient vs immersion time ($C=10^{-3}$ M, $v=0.014$ mms^{-1} , $P_m=90$ MPa). In all cases, the friction coefficient is first measured in pure water, then immediately after introduction of the surfactant. In procedure A, the friction coefficient is measured every 5 min. Procedures B and C are identical to procedure A, but the system is first left at rest for respectively 3 and 15 hours before the friction coefficient measurement starts. With procedures A and B, the friction is initially high and stays constant for some induction period. Low friction is observed immediately after the end of the 15 hour wait period in procedure C.

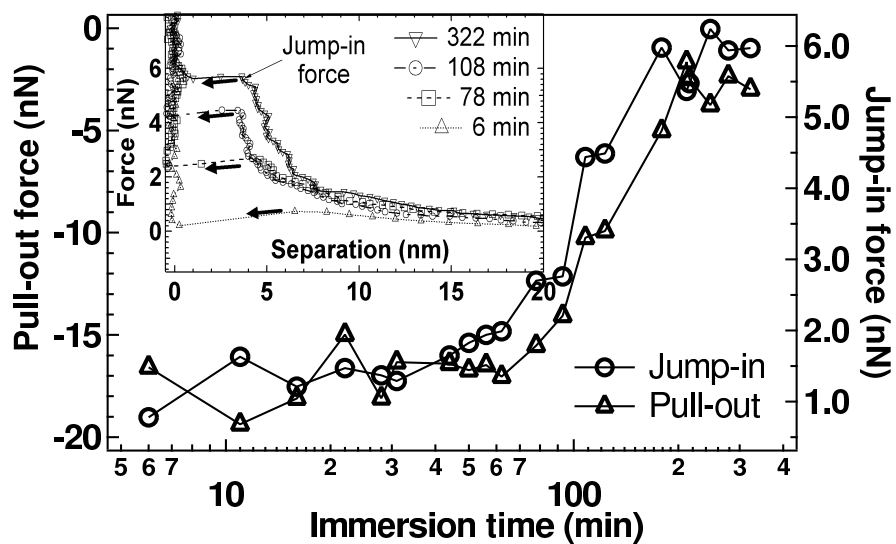


Fig. 7. Time evolution of the jump-in and of the pull-out forces between a silicon nitride tip and a silica surface ($C=1\times 10^{-3}$ M). A few typical force vs distance curves are shown as inset.

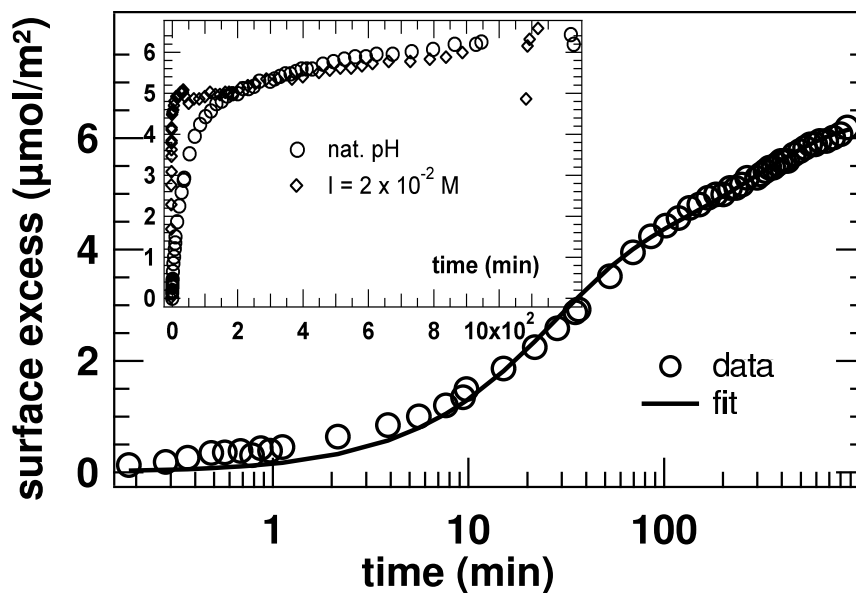


Fig. 8. Adsorption kinetics for DOAIM (5×10^{-4} M) in pure water and fit to a double exponential function ($\tau_1=25$ min, $\tau_2=205$ min). The inset compares the same data with the much faster kinetics at high ionic strength (2×10^{-2} M) on a linear time scale.

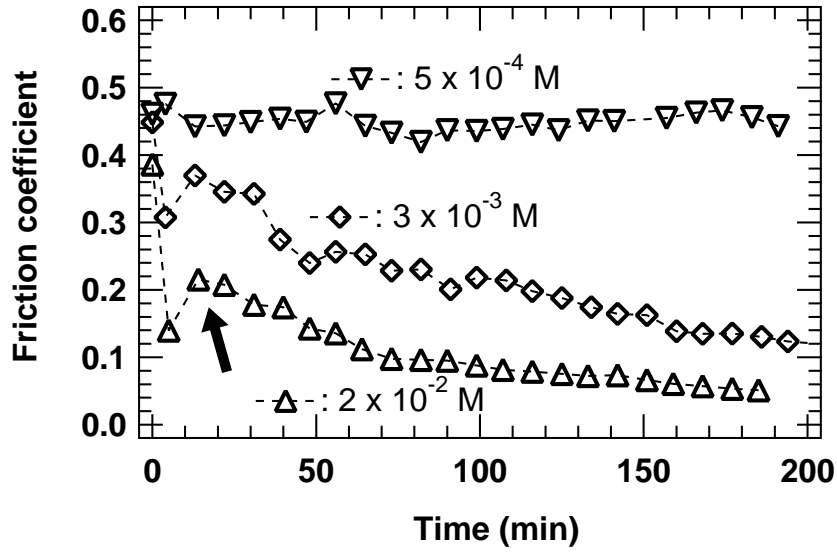


Fig. 9. Evolution of the friction coefficient versus immersion time ($C=5 \times 10^{-4}$ M, natural pH) at different ionic strengths. The arrow points to the friction spike observed after the initial lubrication effect of the surfactant.

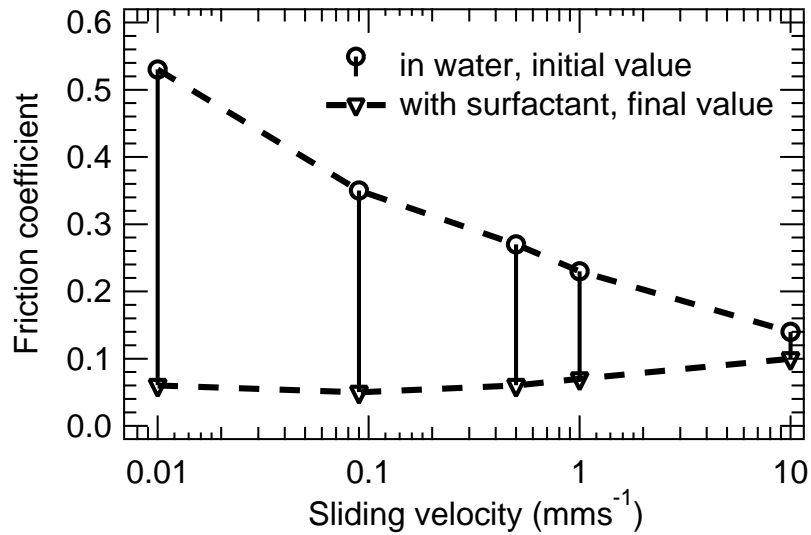


Fig. 10. Impact of shear velocity on the evolution of the friction coefficient between silica surfaces ($C=10^{-3}$ M, $P_m=320-340$ MPa, $v=10$ mms^{-1}).

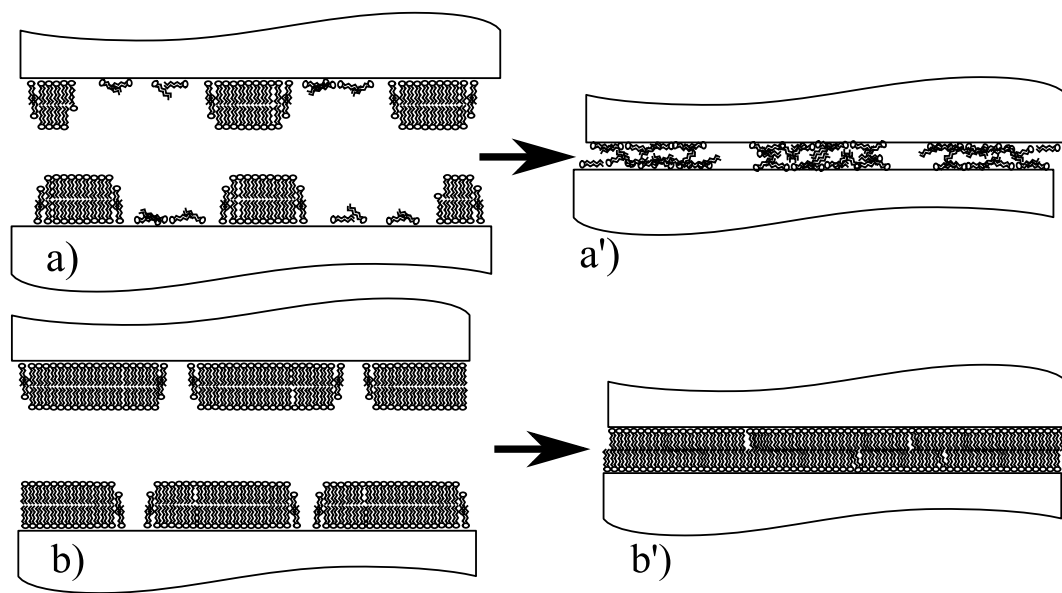


Fig. 11. Schematics of the surfactant instability for a highly defective (a, a') and an almost defect-free (b, b') bilayer.